Peer-reviewed version available at Materials 2017, 10, 1313; doi:10.3390/ma10111313

Article

Selective Laser Sintering of Porous Silica Enabled by Carbon Additive

Shuai Chang[1,2], Liqun Li[1], Li Lu[2] and Jerry Y.H. Fuh [2*]

[1]State Key Laboratory of Advanced Welding and Joining, Harbin Institute of Technology, Harbin 150001, China

[2]Department of Mechanical Engineering, National University of Singapore, Singapore 117576

* Corresponding author: jerry.fuh@nus.edu.sg; Tel.: +65 6516 6690

Abstract: The aim of this study was to investigate the possibility of a freeform fabrication of porous ceramic parts through selective laser sintering (SLS). SLS was proposed to manufacture ceramic green parts because this additive manufacturing technique can be used to fabricate three-dimensional objects directly without a mold, and the technique has the capability of generating porous ceramics with controlled porosity. However, ceramic printing has yet fully achieved its 3D fabrication capabilities without using polymer binder. Except for the limitation of high melting point, brittleness and low thermal shock resistance from instinct ceramic material properties, the key hurdle lies on very poor absorptivity of oxide ceramics to fiber laser which is widely installed in the commercial SLS equipment. An alternative solution to overcome the poor laser absorptivity via improving material compositions was presented in this study. The positive effect of carbon additive on the absorptivity of silica powder to fiber laser will be discussed. To investigate the capabilities of the SLS process, 3D porous silica structures were successfully prepared and characterized.

Keywords: selective laser sintering (SLS); porous ceramic; carbon additive; laser absorptivity

1. Introduction

Advanced ceramic materials offer a high potential for high-end applications due to their unique properties such as high melting point, exceptional mechanical strength, superior wear and thermal resistance, and excellent chemical stability [1, 2]. Tailored porous ceramic exhibits more special features including low thermal mass, low thermal conductivity, high surface area, low density and high specific strength. Therefore, ceramics containing controlled porosity finds nowadays many applications as end products, especially for operation environments where high temperature, extensive wear and corrosive media are involved. Such an increasing number of applications include for example the filtration of hot corrosive gases and molten metals, high-temperature thermal insulation, catalytic carriers in various chemical processes, and membranes for separation and purification [3-5].

Despite of the excellent properties, the wider use of porous ceramics is still limited, because traditional manufacturing processes (e.g., dry pressing, slip casting, tape casting and injection moulding) are time-consuming and shaping through moulding is limited, particularly for complex parts. [6-8]. However, recent developments in additive manufacturing (AM) technologies allows for a rapid freeform fabrication of parts with complex geometries that could be very difficult or even impossible to fabricate by the conventional techniques. AM in general and SLS in particular have recently gained popularity because of its ability to produce complex porous ceramic parts directly without a mold [9]. Manufacturing of complex polymeric or metallic parts directly has been well studied. However, there are very few works on direct selective laser sintering (SLS) of ceramics without using polymer binder. It is still a very challenging task due to the brittleness, low thermal

Peer-reviewed version available at Materials 2017, 10, 1313; doi:10.3390/ma10111313

shock resistance material properties [10, 11]. Besides, the key hurdle for SLS of such materials is that oxide ceramics usually show very poor absorptivity to near-infrared laser [12]. Several researches attempted to obtain direct SLS of ceramics through coating powder with lower-melting point ceramics. But it was still yet achieved since the laser absorptivity of powder coated with some transparent ceramic like silica, laser absorbance is even weaker [13].

Thus this work was aimed to investigate the capabilities of a rapid fabrication of porous ceramic parts via SLS technique. CO_2 laser and Nd:YAG fiber laser are generally used in most of the SLS/M machines. In comparison to Nd:YAG fiber laser emitting at 1,070 nm, CO_2 laser with wavelength of 10.6 μm is much more easier to be absorbed by most of ceramic materials, but the diameter of laser spot is much larger than that of the fiber laser [14, 15]. Therefore, fiber laser is more suited for processing with higher accuracy. However, silica is almost non-absorbent to Nd:YAG fiber [16, 17]. The study on powder absorptivity to laser is aimed to improve the process of the selective laser sintering (SLS) , and it allows one to understand the mechanism of the interaction between laser and materials which is crucial to find a more uniform and suitable processing window for SLS [18]. Therefore, the solution of improving the poor ceramic materials absorptivity to laser was proposed. To investigate the influence of carbon additive to ceramic material, 3D test specimens were successfully fabricated and characterized via the SLS process.

2. Materials and Methods

2.1 Principle of SLS of materials

Selective laser sintering was invented by Carl R. Deckard and Joseph J. Beaman in the 1980s at the University of Texas [18]. The selective laser sintering (SLS) technique as depicted in Fig. 1 is a powder-based additive manufacturing (AM) technique in which a laser beam is used to fuse powder materials selectively according to the digital design of the built part. The CAD/CAM model is sliced into thin layers with thicknesses typically less than 100 μm [19]. Subsequent lowering the building platform a height equating to the layer thickness, followed by additional powder deposition provides a new and free-packed powder layer for a consecutive melting step. These repeating steps allow for generation of three-dimensional complex and near-net-shaped parts.

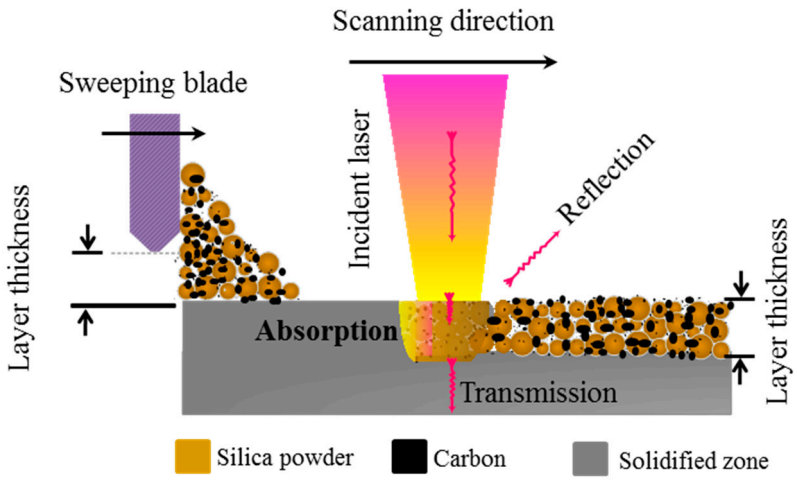

Figure 1. Schematic drawing of laser impinging on the powder bed in SLS process.

The intrinsic feature of laser processing of ceramics is that, at a certain time of interaction between the laser beam and ceramic powder bed, only a little laser energy is absorbed; some is transmitted and the rest is reflected away as depicted in Fig. 1. To evaluate the efficiency of laser processing, it is necessary to know how much of the incident laser intensity is coupled to the

Peer-reviewed version available at Materials 2017, 10, 1313; doi:10.3390/ma10111313

sample. This coupling efficiency is described by "absorptance" (this is also referred to as absorption coefficient or just absorption). Other quantities often used to evaluate the laser processing are called *reflectance* and *transmittance*. The delineations of these quantities are given as follows. The absorptance, *A*, is given by:

$$A = 1 - T - R \quad (1)$$

$$A = \text{(Absorbed laser energy in the sample) / (Total incident laser power)} \quad (2)$$

while reflectance, *R*, is

$$R = \text{(Reflected laser energy from the sample) / (Total incident laser power)} \quad (3)$$

and transmittance, *T*, is defined by,

$$T = \text{(Transmitted laser energy through the sample) / (Total incident laser power)} \quad (4)$$

In this study, reflectance (*R*) and transmittance (*T*) will be measured.

2.2 Materials and samples preparation

Silica powder (SS1206, Industrial Powder, USA) was used for this study. This silica powder is in spherical shape (Fig. 2). As shown in Fig. 3, the particle size is distributed from 1μm to 60 μm (measured by laser diffraction on LS 100 Q, Coulter International Corporation, USA). Fine active carbon powder with the weigh radio of 0.1% - 0.3 % was doped into silica powder to increase the laser absorptivity. The composite particles were mechanically mixed with Ball Mill (from Planetary Mono Mill, FRITSCH GmbH, Germany) at 150 rpm for 10 hours. The powder was dried in a drying oven at 80°C for two hours before SLS process.

The SLS machine used in the present work is a self-developed SLS system. It is equipped a fibre laser (P_{max} = 200 W c.w.) with a wavelength of 1,070 nm and a laser beam focusing diameter of ~ 100 μm. It is comprised a 100 × 100 × 150 mm^3 build envelope and the powder layer was deposited by blade. The whole process was conducted under the air atmosphere.

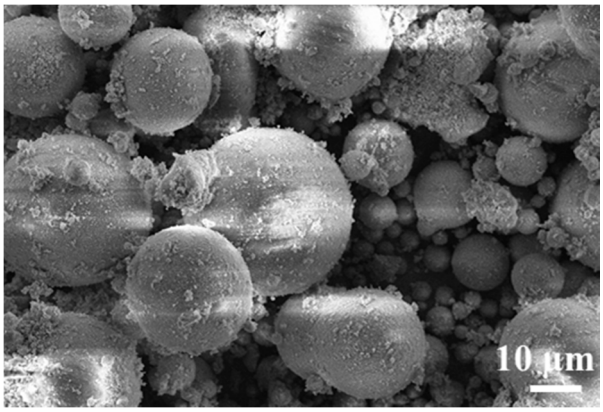

Figure 2. Morphology of original silica (SiO_2) powder.

Preprints (www.preprints.org) | NOT PEER-REVIEWED | Posted: 1 October 2017 doi:10.20944/preprints201710.0003.v1

Peer-reviewed version available at Materials 2017, 10, 1313; doi:10.3390/ma10111313

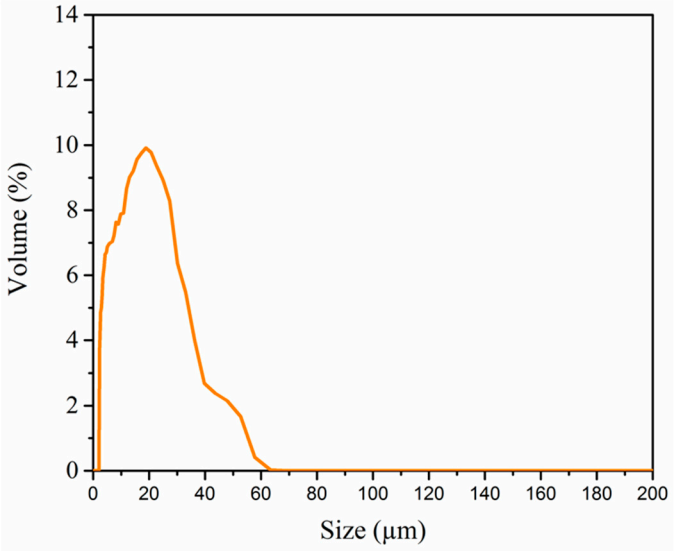

Figure 3. Particle size distribution of the spherical silica powder.

The main parameters for the SLS processing are illustrated in Fig. 4, including : (1) laser power (P); (2) hatch distance (HD); (3) scan speed (v); (4) laser spot size (D); (5) layer thickness (T); and (6) scanning strategy. Optimized SLS parameters shown in Table. 1 were applied to fabricate green specimens with a set-up dimension of 8 × 8 mm^2 for investigations in this study.

In order to increase the bonding of the SLS parts, the furnace sintering was applied in a high temperature chamber furnace (Carbolite HTF 17/5/3216P1, UK). The parts were heated at 2 °C/min in air to 1,200 °C for 5h. The whole furnace sintering process is much more cost-effective and less time consuming owning to omission of de-binding process, because the raw material is free of polymer binder.

2.3 Measurements

The morphology of the specimens was observed by optical microscope (OLYMPUS SZX10) and scanning electron microscopy (SEM, JEOL JSM5510LV) equipped with energy dispersive X-ray spectroscopy (EDX, Oxford 7582). The crystal structure was characterized by X-ray diffraction (XRD-6000 Cu-Ka radiation, Shimadzu). Thermogravimetric analysis and differential thermal analysis (DTA) (DTA-TG, Shimadzu DTG-60H) were used in the range from room temperature to 1,400 °C in a flowing air atmosphere with a heating rate of 5 °C/min. The UV–vis-NIR spectra were obtained with a Cary 5000 UV–vis-NIR spectrophotometer. X-ray CT scan of the printed part is carried out by using high-resolution XCT system Phoenix Nanotom® m. The density was measured by the Archimedes' method in water. To calculate the amount of shrinkage of the SLS parts, the dimension of cubic parts was measured by digital vernier caliper.

Table 1. Optimized laser sintering parameters

Laser power (W)	Hatch space (μm)	Scan speed (mm/s)	Spot size (μm)	Layer thickness (μm)
60	150	50	120	90

Preprints (www.preprints.org) | NOT PEER-REVIEWED | Posted: 1 October 2017 doi:10.20944/preprints201710.0003.v1

Peer-reviewed version available at Materials 2017, 10, 1313; doi:10.3390/ma10111313

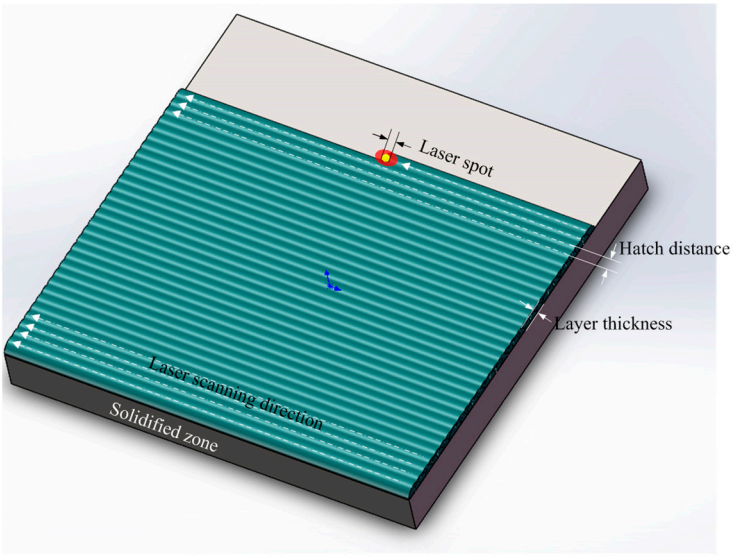

Figure 4. Key parameters in the SLS process.

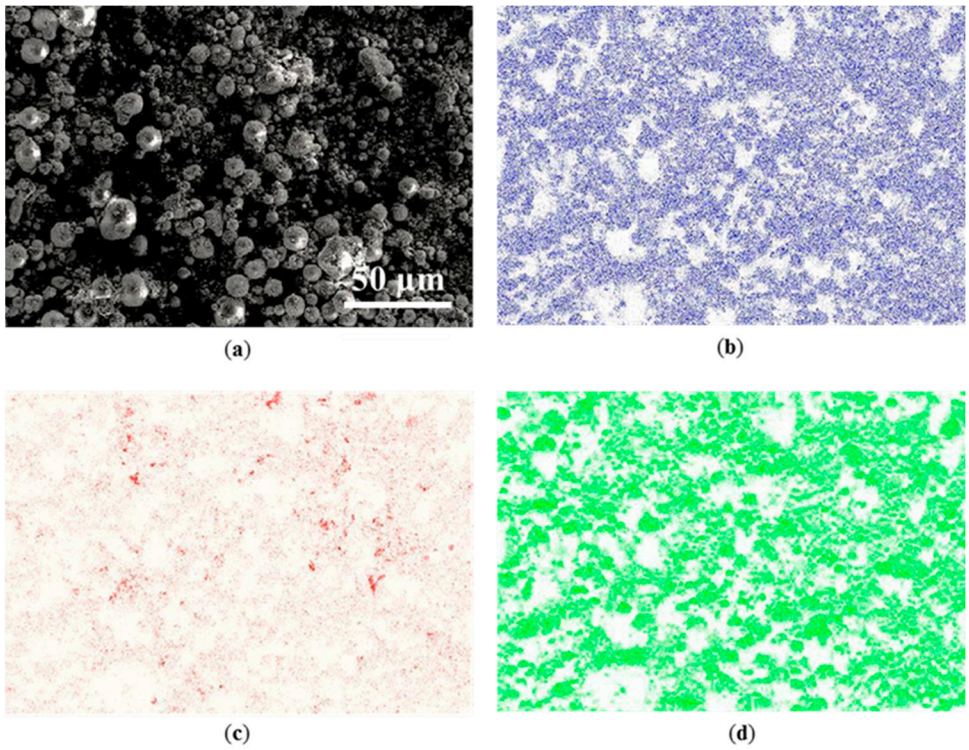

Figure 5. Micrographs showing characteristic distribution of silica powder with 0.2 wt.% of carbon additive. (a) SEM micrograph of mixed powders. The corresponding EDX mapping images of (b) silicon, (c) carbon and (d) oxygen elements.

3. Results and Discussions

SEM micrograph and EDX analyses of silica powder with carbon addition were carried out as a loose powder bed (Fig. 5). The ball mill at low rotating speed has achieved uniform mixing without crushing spherical silica granules (Fig. 5(a)) The overall EDX mapping of powder bed demonstrates that the powder contain primarily carbon (C), silicon (Si) and oxygen (O). No traces of other elements were found. This confirms that powder was not contaminated during ball milling process. The distribution of carbon is well consistent with that of silicon and oxygen elements, which indicates that C distributes uniformly on the micron-size particles.

Preprints (www.preprints.org) | NOT PEER-REVIEWED | Posted: 1 October 2017 doi:10.20944/preprints201710.0003.v1

Peer-reviewed version available at Materials 2017, 10, 1313; doi:10.3390/ma10111313

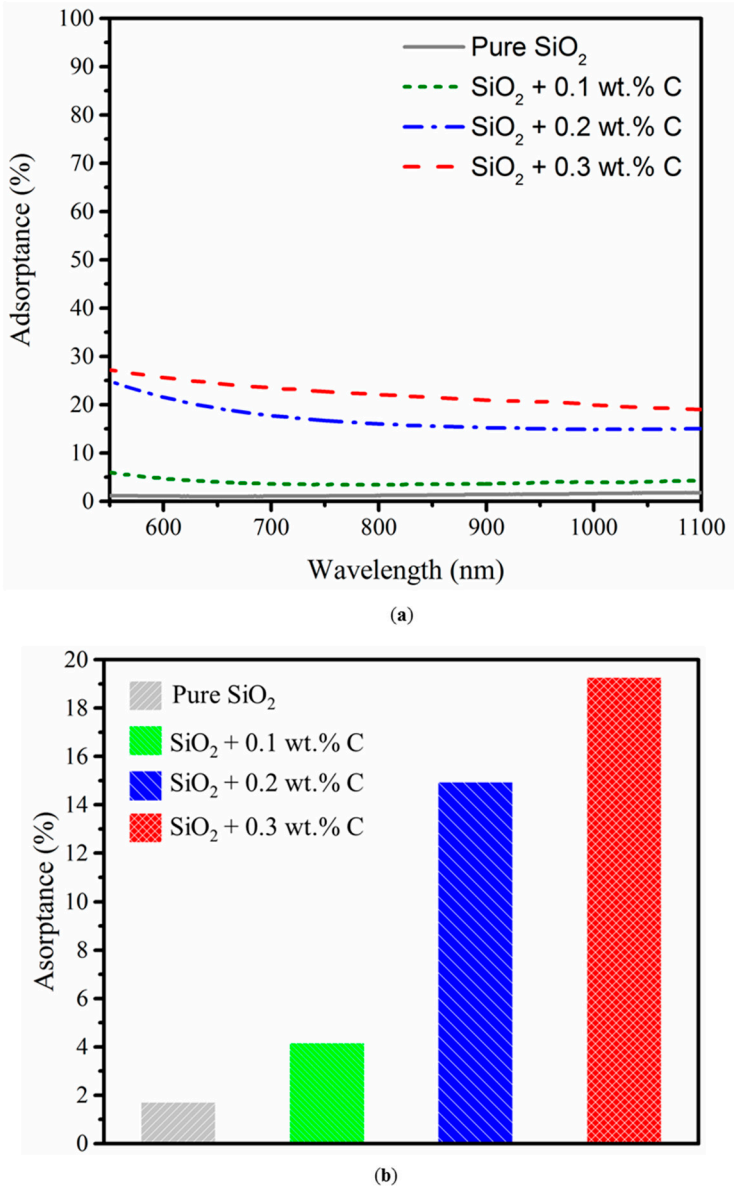

Figure 6. Comparison of absorptance to near-infrared light with varied amount of carbon additive. (a) UV–vis-NIR absorption spectra; (b) absorptance to UV light at1,070 nm wavelength.

As introduced previously, fine carbon was doped into the silica granules to enhance the absorptivity to laser beam. The absorptance of silica powder measured for different carbon doping quantity was presented in Fig. 6. The UV–vis-NIR absorption spectra was measured on green pellet with the thickness of 4mm, which shows the clear improvement of absorptance by increasing amounts of carbon additive (Fig. 6(a)). Comparison of the absorptance to fiber laser (λ =1,070 nm) in pellets containing different amount of the additive reveals significant changes (Fig. 6(b)). The absorptance at 1,070nm wavelength of SiO_2+ 0.1 wt.% C, SiO_2 + 0.2 wt.% C and SiO_2 + 0.3 wt.% C has reached to ~4%, ~16% and ~19%, respectively. The absorbance to fiber laser of SiO2 + 0.2 wt.% C is up to 8 times higher than pure silica.

The significant benefit from doped carbon was revealed in the comparison of SLS of silica with different carbon addition (Fig. 7). The one-layer samples shown in Fig. 7 were all prepared under same process parameters, which are listed in Table 1. It is evident that the conditions of powder melting with varied carbon addition are different. The ceramic powders with carbon were at least joined to form a solid piece with the absorption of laser energy. However, there was almost no any

Peer-reviewed version available at Materials 2017, 10, 1313; doi:10.3390/ma10111313

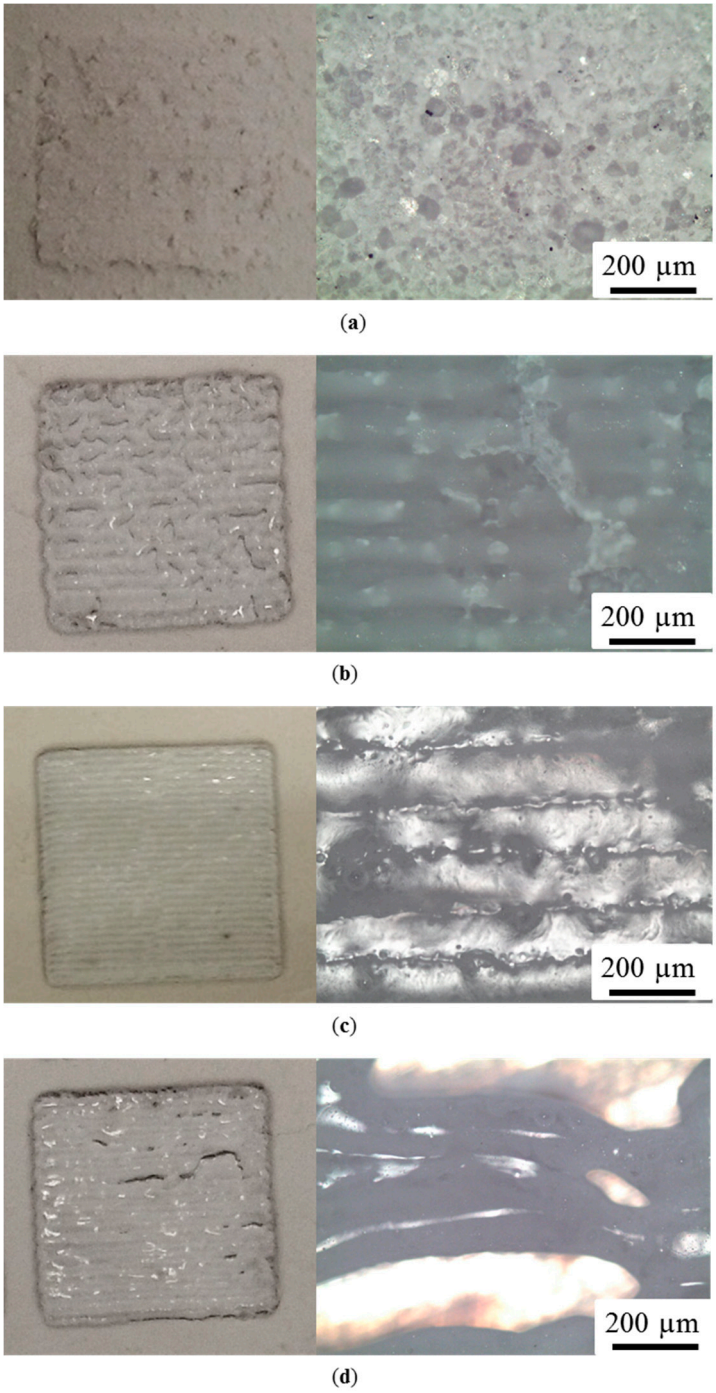

Figure 7. Optical graphs showing the appearance and cross-section of SLS sample surface with varying the amount of carbon additive. (a) pure silica; (b) silica + 0.1 wt.% carbon; (c) silica + 0.2 wt.% carbon; (d) silica + 0.3 wt.% carbon.

trace of melting in the pure silica powders because of poor absorptivity. It is worth to mention that unsuitable amount of the carbon additive would introduce macro-cracks (Fig. 7(d)) owing to the excess doping and the insufficient doping may result in uncontentious joining (Fig. 7(b)). In the range of the studied amount of carbon additive, good quality of melting and bonding without visible cracks was formed by doping 0.2 wt.% of carbon (Fig. 7(c)).

Along with doping small amount of carbon, the laser absorptivity at 1,070nm was obviously enhanced. On the other hand, it was proved that no reaction between active carbon as shown in the X-ray diffraction (XRD) results (Fig. 8). The X-ray diffraction pattern revealed that the structures are well crystallized into quartz phase after laser sintering. The transformation of quartz into

Peer-reviewed version available at Materials 2017, 10, 1313; doi:10.3390/ma10111313

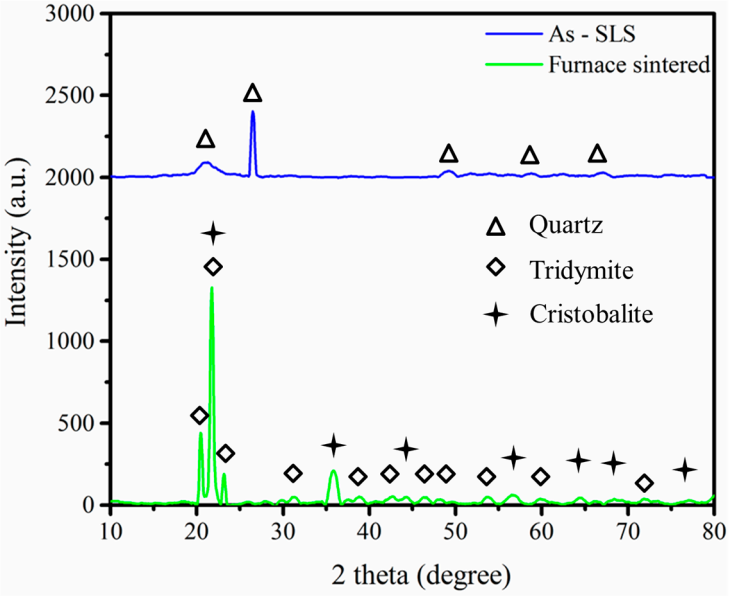

Figure 8. XRD pattern of as-SLS green part and final sintered part.

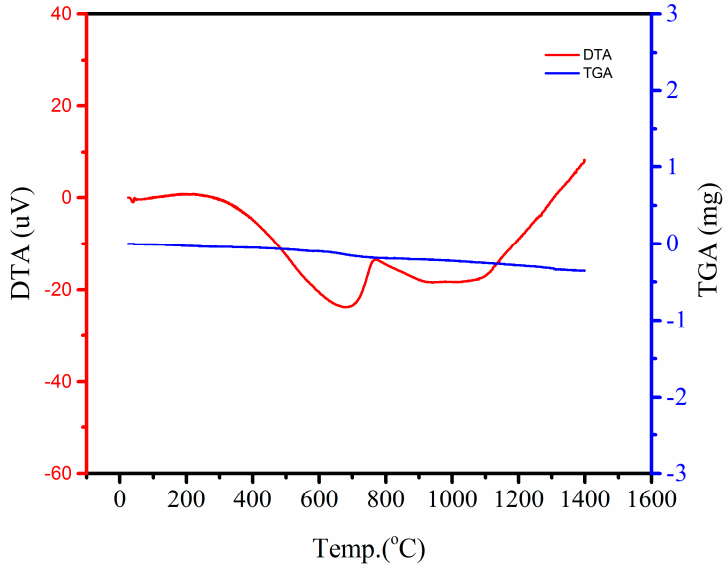

Figure 9. DTA/TGA curve of the silica powder with 0.2 wt% of carbon additive.

cristobalite and tridymide after furnace sintering was also analyzed. There is no carbon phase or any composite phase detected in both green and final ceramic parts as a consequence of carbon addition. Hence, there is no risk to induce undesirable contamination or new phase which may have negative effects on the final properties. The carbon may be consumed by the reaction with the oxygen in the air, which will contribute some heat energy to the SLS process. This thermal behavior of the carbon additive is shown by the DTA/TGA curve (Fig. 9).

The good melting and bonding is the prerequisite to create porous structures. One efficient way of generating the porous part is to enlarge the hatch distance (*H*). In this case, the particles would bond together but void could be left inside. Therefore, the porosity can be tailored by varying *H*. Fabrication of 3D porous silica part has been conducted with optimized parameters and lager hatch distance (300μm) according to Table 1. Porous silica cubic sample with twenty layers (Fig. 10) was successfully fabricated via SLS followed by furnace sintering. Defects such as cracks were not observed in the cross section of the sample (Fig. 10 (c)). Continuous pores with random distribution were formed between the particles which bonded in necking mechanism (Fig. 10 (d)). The successful fabrication of silica containing tailored porosity was also demonstrated in the 3D

Peer-reviewed version available at *Materials* **2017**, *10*, 1313; doi:10.3390/ma10111313

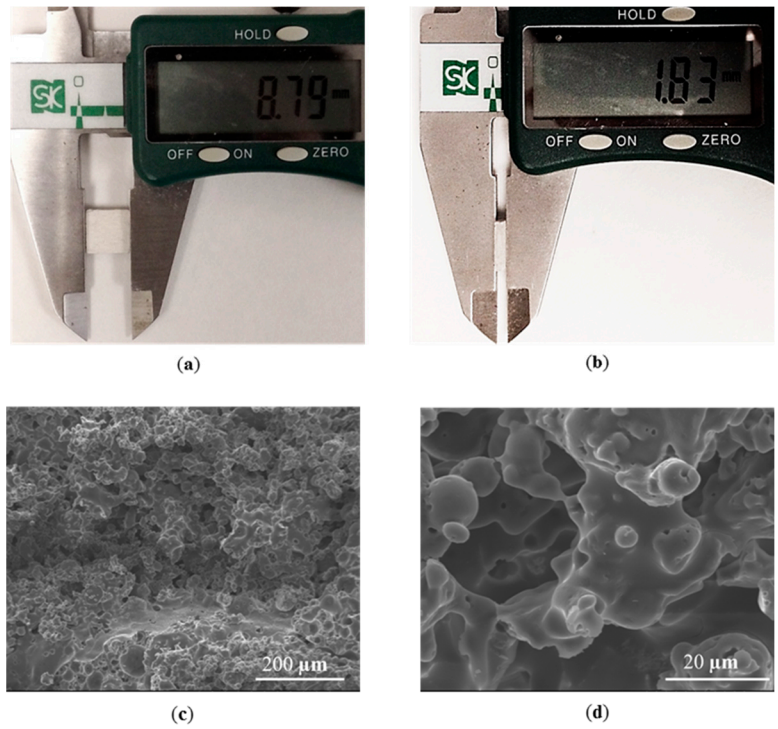

Figure 10. Silica part produced by the SLS + sintering. (a) top view of the silica cubic; (b) side view of the silica cubic. SEM micrographs of fracture surface of final sintered sample. (c) low-magnification; (d) high- low-magnification.

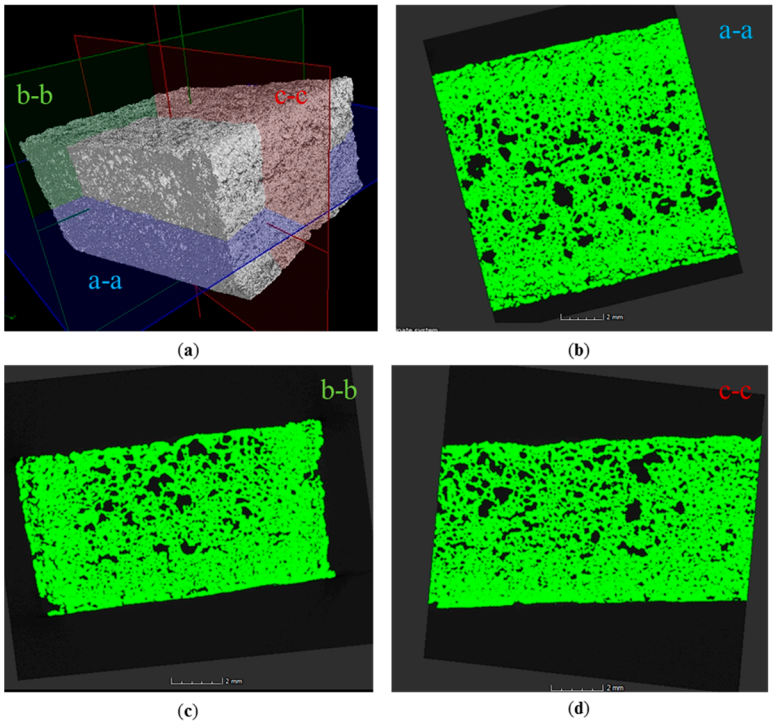

Figure 11. Image renderings from micro-CT scans of final porous silica specimen produced by SLS. (a) 3D image; (b) cross-section parallel to the building direction; (c) cross-section vertical to laser scanning direction; (d) cross-section parallel to laser scanning direction

reconstruction from micro-CT scan (Fig. 11). The linear and volume shrinkage: ΔL/L, ΔW/W, ΔH/H and ΔV/V, were measured by digital Vernier caliper, and the results were 1.45%, 1.57%, 2.7% and 6.75% in length, width,

height and volume, respectively. An excellent bonding and low shrinkage of the porous silica structure was obtained owing to direct SLS with carbon additive and without the use of polymer binder in laser sintering.

4. Conclusions

In this paper, the capabilities of manufacturing porous silica by means of selective laser sintering (SLS) without using polymer binder have been demonstrated. The significant improvement of laser absorptivity by doping carbon to silica material has been highlighted. Furthermore, there is no trace of undesirable contamination or new phase which may result in negative effects on the final properties. The well-bonded 3D porous silica structure with low shrinkage was successfully fabricated without visible defects. Moreover, this approach is also applicable to fabricate other porous ceramic parts through laser sintering. The material processing technique although is time-consuming, it makes direct SLS of porous silica structure possible.

Acknowledgments: The work described in this paper was jointly supported by the overseas exchange of NUS-HIT, NUS Strategic Research Programme fund and Morgan Advanced Materials Pt Ltd, Singapore

Author Contributions: Shuai Chang and Jerry Ying Hsi Fuh conceived and designed the experiments; Shuai Chang, Liqun Li and Li Lu analyzed the material data. Shuai Chang performed the experiments and wrote the paper.

Conflicts of Interest: The authors declare no conflict of interest.

References

1. Liang, Y.H.; Sourin P.D. Application trend in advanced ceramic technologies. *Technovation* **2001,** 21, 61-65.
2. Ohmura, A.; Ouchi, N.; Morisaki, S.; Watanabe, C. Functionality development as a survival strategy for fine ceramics. *Technovation* **2003**, 23, 833-842.
3. Scheffler, M.; Colombo, P. Cellular ceramics: structure, manufacturing, properties and applications. *John Wiley & Sons* **2006.**
4. Gauckler, L.J.; Waeber, M.M.; Conti, C.; Jacob-Duliere, M. Ceramic foam for molten metal filtration. *JOM Journal of the Minerals, Metals and Materials Society* **1985**, 37, 47-50.
5. Tang, H.H.; Chiu, M.L.; Yen, H.C. Slurry-based selective laser sintering of polymer-coated ceramic powders to fabricate high strength alumina parts. *J. Eur. Ceram. Soc.* **2011**, 31, 1383-1388.
6. Wu, H.; Li, D., Tang, Y.; Sun, B.; Xu, D. Rapid fabrication of alumina-based ceramic cores for gas turbine blades by stereolithography and gelcasting. *J. Mater. Process. Technol.* **2009**, 209, 5886-5891.
7. Travitzky, N. Processing of ceramic–metal composites. *Advances in Applied Ceramics* **2012**,111, 286-300.
8. Kruth, J.P.;Leu, M.C.;Nakagawa, T. Progress in additive manufacturing and rapid prototyping. *CIRP Ann. Manuf. Technol.***1998**, 47, 525-540.
9. Bertrand, P.; Bayle, F.; Combe, C.; Gœuriot, P.; Smurov, I. Ceramic components manufacturing by selective laser sintering. *Appl Surf Sci.* **2007,** 254, 989-992.
10. Shishkovsky, I.; Yadroitsev, I.; Bertrand, P.; Smurov, I.; Alumina–zirconium ceramics synthesis by selective laser sintering/melting. *Appl Surf Sci.* **2007,** 254, 966-970.
11. Tolochko, N.K.; Khlopkov, Y.V.; Mozzharov, S.E.; Ignatiev, M.B.; Laoui, T.; Titov, V.I. Absorptance of powder materials suitable for laser sintering. *Rapid Proto J.* **2000**, 6, 155-161.
12. Kruth, J.P.; Levy, G.; Klocke, F.; Childs, T.H.C. Consolidation phenomena in laser and powder-bed based layered manufacturing. *CIRP Ann. Manuf. Technol* **2007**, 56, 730-759.
13. Gahler, A.; Heinrich, J.G.; Guenster, J. Direct Laser Sintering of Al2O3–SiO2 Dental Ceramic Components by Layer-Wise Slurry Deposition. *J. Am. Ceram. Soc.* **2006,** 89, 3076-3080.
14. Qian, B.; Shen, Z. J. Laser sintering of ceramics. *Asian Ceram. Soc.* **2003,** 1, 315-321.

15. Juste, E.; Petit, F.; Lardot, V.; Cambier, F. Shaping of ceramic parts by selective laser melting of powder bed *J Mater Res.* **2014,** 29, 2086-2094.
16. Duley, W. Laser processing and analysis of materials. *Springer Science & Business Media* **2012**.
17. Beaman, J. J.; Deckard, C. R. Selective laser sintering with assisted powder handling. *U.S. Patent* **1990**.
18. Ko, S.H.; Pan, H.; Grigoropoulos, C.P.; Luscombe, C.K.; Fréchet, J.M.; Poulikakos, D. All-inkjet-printed flexible electronics fabrication on a polymer substrate by low-temperature high-resolution selective laser sintering of metal nanoparticles. *Nanotechnology*. **2007**, 18, 345.
19. Kruth, J.P.; Vandenbroucke, B.; Vaerenbergh, V.J.; Naert, I. Rapid manufacturing of dental prostheses by means of selective laser sintering/melting *Proc. AFPR*. **2005**.